NEOPLASIA
www.neoplasia.com

Volume 15 Number 5 May 2013 pp. 461–471 461

PTEN Deficiency Contributes to the Development and Progression of Head and Neck Cancer[1]

Cristiane H. Squarize*, Rogerio M. Castilho*, Aline C. Abrahao†, Alfredo Molinolo‡, Mark W. Lingen§ and J. Silvio Gutkind‡

*Laboratory of Epithelial Biology, Department of Periodontics and Oral Medicine, University of Michigan, Ann Arbor, MI; †Department of Pathology and Oral Diagnosis, Federal University of Rio de Janeiro School of Dentistry, Rio de Janeiro, RJ, Brazil; ‡Oral and Pharyngeal Cancer Branch, National Institute of Dental and Craniofacial Research, National Institutes of Health, Bethesda, MD; §Department of Pathology, The University of Chicago, Chicago, IL

Abstract

The sequencing of the head and neck cancer has provided a blueprint of the most frequent genetic alterations in this cancer type. They include inactivating mutations in *Notch*, *p53*, and $p16^{ink4a}$ tumor suppressor genes, in addition to nonoverlapping activating mutations of the *PIK3CA* and *RAS* oncogenes or inactivation of the tumor suppressor gene *PTEN*. Notably, these genetic alterations, along with epigenetic changes, result in increased activity of phosphoinositide 3-kinase (PI3K)/AKT/mammalian target of rapamycin (mTOR) pathway, which is present in most head and neck squamous cell carcinomas (HNSCCs). Moreover, we show here that approximately 30% of HNSCCs exhibit reduced PTEN expression. We challenged the biologic relevance of this finding by combining the intraoral administration of a tobacco surrogate, 4-nitroquinoline 1-oxide, with a genetically defined animal model displaying reduced PTEN expression, achieved by the conditional deletion of *Pten* using the keratin promoter 14 CRE-lox system. This provided a specific genetic and environmentally defined animal model for HNSCC that resulted in the rapid development of oral-specific carcinomas. Under these experimental conditions, control mice did not develop HNSCC lesions. In contrast, most mice harboring *Pten* deficiency developed multiple SCC lesions in the lateral border and ventral part of the tongue and floor of the mouth, which are the preferred anatomic sites for human HNSCC. Overall, our study highlights the likely clinical relevance of reduced PTEN expression and/or inactivation in HNSCC progression, while the combined *Pten* deletion with exposure to tobacco carcinogens or their surrogates may provide a unique experimental model system to study novel molecular targeted treatments for HNSCC patients.

Neoplasia (2013) 15, 461–471

Introduction

Head and neck squamous cell carcinomas (HNSCCs) represent one of the 10 most common cancers worldwide [1]. Tobacco and alcohol consumption are well-known risk factors for this cancer type, along with the recently described involvement of human papillomavirus infection [1–3]. Although very rarely diagnosed in the early stages, the survival rate for early diagnosed HNSCC patients is approximately 82.4% within the first 5 years, whereas for late-stage HNSCC the survival rate drops to 34.9% according to the National Cancer

Address all correspondence to: Cristiane H. Squarize, DDS, MS, PhD, University of Michigan, 1011 N University Ave., Room 3210, Ann Arbor, MI 48109-1078.
E-mail: csquariz@umich.edu

[1]This work was supported by the Intramural Research Program, National Institute of Dental and Craniofacial Research, National Institutes of Health (NIH) and the University of Michigan Comprehensive Cancer Center through grant P50-CA97248 (University of Michigan Head and Neck, Specialized Programs of Research Excellence) from the NIH/National Cancer Institute. A.C.A. was supported by Coordenação de Aperfeiçoamento de Pessoal de Nível Superior (Brasília, DF, Brazil).
Received 25 June 2012; Revised 19 February 2013; Accepted 20 February 2013

DOI 10.1593/neo.121024

Institute Surveillance Epidemiology and End Results (www.seer.cancer.gov). An additional factor influencing survival is the development of multiple primary tumors that are also associated to field cancerization and chronic tobacco exposure, constituting the most common cause of treatment failure and death among early-stage patients [1,2,4].

Although some of the genetic and epigenetic events underlying this complex disease have been identified [5,6], the molecular pathways involved in HNSCC tumor development and progression are still poorly understood. Recently, the genome-wide sequence analyses of HNSCC have enlightened the field by defining its most frequent somatic genetic alterations [5,6]. Interestingly, a large number of mutations were identified, which include the known *TP53* and *HRAS* mutations and other previously unrecognized ones, such as mutations in the NOTCH family genes (*NOTCH1*, *NOTCH2*, and *NOTCH3*). These multiple mutations confirmed the heterogeneity of the HNSSC tumors, which is reflected in the diverse biology, response to treatment, and prognosis of HNSCC patients. Additionally, several mutations were identified in the phosphoinositide 3-kinase (PI3K)/mammalian target of rapamycin (mTOR) pathway, including *PIK3CA* (8–10%), *TSC1/2* (5–8%), and *PTEN* (5–10%) [5–8], all of which result in PI3K/AKT/mTOR pathway activation. Detailed exon sequencing in one study revealed *PTEN* mutations in up to 23% of the tumor samples [7]. In particular, loss of chromosome 10 and missense mutations were identified in *PTEN* exons 5, 6, 7, and 8 [7]. Furthermore, mutations present in the same pathway are rarely reported in the same tumor [6,9,10], which underscores the importance of these pathways in the pathophysiology of this disease. However, not necessarily all the genetic alterations identified by high-throughput sequencing approaches are driver mutations, and clearly new approaches are needed to better understand the biologic relevance of these mutations and, hence, their contributions to the molecular pathways involved in HNSCC initiation and progression.

By combining our engineered animal models of HNSCC to a relevant chemical carcinogenesis approach using 4-nitroquinoline 1-oxide (4NQO), we have now developed an oral specific HNSCC animal model that allowed us to study the different molecular, biologic, and clinical aspects of HNSCC. This novel animal model closely recapitulates human HNSCC progression and, hence, enabled us to analyze the contribution of the activation of PI3K/AKT/mTOR pathway and *PTEN* deregulation/deactivation and mutations to the development of HNSCC. We started by deleting *Pten* selectively from the proliferative epithelial layer using the Cre system driven by the cytokeratin 14 promoter (K14Cre). PTEN is a phosphatase that hydrolyzes phosphatidylinositol 3,4,5-trisphosphate (PIP_3) to phosphatidylinositol 4,5-bisphosphate (PIP_2), hence representing a key negative regulator of the PI3K/AKT/mTOR pathway [11,12]. Thus, deactivation and/or down-regulation of PTEN due to mutations, epigenetic changes, or posttranslational regulation can be recapitulated by the partial (heterozygous) or complete (homozygous) deletion of the *Pten* gene, which results in the activation of PI3K pathway. These mice were also exposed to a tobacco surrogate, 4NQO, which leads to the development of oral lesions and malignant transformation within the oral cavity, similar to that observed in humans. Our animal model closely mimics the human disease and can be effectively used for future preclinical studies. Overall, our study shows the importance of the PI3K/AKT/mTOR and PTEN to HNSCC initiation and progression and, thus, supports a critical role of this pathway in a subset of HNSCC patients.

Materials and Methods

Genetically Defined HNSCC Animal Model

All animal studies were carried out according to an institutionally approved protocol, in compliance with the Guide for the Care and Use of Laboratory Animals. K14Cre $Pten^{F/F}$ mice were obtained by crossing as previously described [13,14] to generate K14Cre $Pten^{F/+}$ (heterozygous deletion), K14Cre $Pten^{F/F}$ (homozygous deletion), and control mice in the same litter. The mice had free access to water and pellet stock diet, with the addition of high-fat supplement, when needed. Genotyping was performed from tail biopsies using a polymerase chain reaction assay as previously described [13]. 4NQO (Sigma-Aldrich, St Louis, MO) was diluted in initially dissolved propylene glycol (4 mg/ml). Sixty 5-week-old littermates were divided into groups of 10 animals and exposed to vehicle or 4NQO (50 μg/ml) in drinking water for 13 weeks. As previously described, water was changed weekly allowing minimal intervention [15]. The animals were killed at the end of the study for final examination and tissue collection. For gene excision analysis, reporter mice was obtained by crossing K14Cre transgenic mice to ROSA26 (R26R) mice [16] containing a *LacZ* gene flanked by loxP sites (ROSA-floxed-lacZ mice).

Histology and Immunohistochemistry of Tissue Microarrays and Tissue Sections

Hematoxylin and eosin (H&E) staining was performed on formalin-fixed and paraffin-embedded 4-μm serial sections according to standard procedures. Immunohistochemistry was performed on these paraffin-embedded tissue sections as described previously [13,17]. Two distinct sets of tissue microarrays (TMAs) containing 711 HNSCC (cores) of normal adjacent oral epithelium, oral dysplasia, and HNSCC were obtained from the National Institute of Dental and Craniofacial Research (NIDCR), National Institutes of Health (Bethesda, MD; $n = 347$) [18] and from the University of Chicago ($n = 362$ HNSCC and 102 normal/dysplasias). For immunohistochemical reaction, antibodies against PTEN (Cascade Bioscience, Winchester, MA), $pAKT^{Ser473}$, $pAKT^{Thr308}$, pS6, epidermal growth factor receptor (EGFR; Dako, Carpinteria, CA), $pEGFR^{Tyr1068}$, and p53 (Cell Signaling Technology, Danvers, MA) were used. According to the immunoreactivity, the tissue array sample cores were classified into five groups: 0 (less than 10% stained cells), 1 (from 10% to 25% of stained cells), 2 (from 25% to 50% of stained cells), 3 (from 50% to 75% of stained cells), and 4 (from 75% to 100% of stained cells. PTEN expression was also classified as negative (group 0 or less than 10% stained cells) and positive (groups 1–4 or 10% to 100% of stained cells). Immunostainings and H&E stains were assessed by two experienced pathologists. Animals from both cohorts (4NQO and vehicle) were analyzed, and detailed histopathologic analyses were performed in each animal at the end of the study. Lesions were classified as normal, hyperplasias, dysplasias (premalignant lesions), and carcinomas (all malignant tumors, including carcinomas *in situ*). Images were taken using the ScanScope CS System (Aperio Technologies, Inc, Vista, CA) and QImaging EXi Aqua monochrome digital camera and Nikon Eclipse 80i Microscope (Nikon, Melville, NY). Hierarchical clustering analysis were done using the Cluster program with average linkage based on unsupervised clustering analysis as the selection variable and visualized using the TreeView program. The biomarkers with a close relationship are located next to each other.

Cancer Microarray Database and Data Mining Platform

Oncomine (Compendia Bioscience, Ann Arbor, MI) [19] was used for retrieving the public cancer database information for the analysis of cancer genes and HNSCC. By the use of the Oncomine data analysis package, the relationship between alterations in PTEN mRNA expression levels and lymph node involvement (N0, no lymph node invasion, and N1+, lymph node invasion in one or more lymph nodes) were retrieved from the head and neck study of Ginos et al. [20], and the results were also confirmed with data from head and neck studies of Cromer et al., Chung et al., and O'Donnell et al. [21–23].

β-Galactosidase Assay

Frozen sample sections (5–6 μm) were fixed with 0.2% glutaraldehyde for 2 minutes and washed multiple times in 1× phosphate-buffered saline. Cryosections were stained with X-Gal solution (2 mg/ml X-Gal). Staining was performed in the dark at 37°C for 6 to 8 hours, mounted in 80% glycerol, and visualized by differential interference contrast microscopy, also known as Nomarski Interference Contrast, using a Zeiss Axiophot microscope [24].

Primary Culture of Keratinocytes and Immunoblot

Murine keratinocytes were isolated and grown in KBM-2 medium (Cambrex, East Rutherford, NJ) as previously described [14]. After lyses, protein concentrations were determined and 30 μg of proteins was separated on 10% sodium dodecyl sulfate–polyacrylamide gel electrophoresis, transferred to nitrocellulose membranes, blocked with 5% milk protein, and incubated with primary antibodies anti-PTEN (Cascade Bioscience) and tubulin (Santa Cruz Biotechnology, Dallas, TX) as previously described [13].

Immunofluorescence and Immunohistochemistry in Mouse Tissues

Immunofluorescence was performed on 5-μm-thick tissue sections. The standard procedure was used to dewax and hydrate the tissues through graded alcohol followed by antigen retrieval and endogenous peroxidase block. Antibody against pS6 (Cell Signaling Technology) was incubated at 4°C and overnight in 3% BSA. Fluorescein isothiocyanate–conjugated secondary antibody (Jackson ImmunoResearch Laboratories, West Grove, PA) was added as described previously [14]. Microvessel density was determined following identification of blood vessels with a polyclonal anti-human factor VIII antibody (Lab Vision, Fremont, CA). For nuclear staining, Hoeschst 33342 or mounting medium with 4′,6-diamidino-2-phenylindole (DAPI; Vector Laboratories, Burlingame, CA) was used. Antibodies used for immunohistochemistry performed in mouse tissue were anti–COX-2 (BD Transduction Laboratories, San Jose, CA) and pAKT (Cell Signaling Technology). Images were taken using Zeiss Axio Imager Z1 microscope equipped with an Apotome device (Carl Zeiss, Thornwood, NY) and ScanScope (Aperio Technologies, Inc).

Statistical Analysis

Statistical analysis was carried out using GraphPad Prism 5.00 (GraphPad Software, San Diego, CA). The analysis of variance followed by Bonferroni multiple comparison test and Student's *t* test was used. Dunn multiple comparison test was used for lesion size. Significant differences between two groups were noted by asterisks or actual *P* values [$^{*}P \leq .05$, $^{**}P \leq .01$, $^{***}P \leq .001$, and NS ($P > .05$, not significant)].

Results

PTEN Down-Modulation Is Associated with Tumor Progression and Aggressive Behavior in HNSCC Patients

We started by defining the levels of PTEN expression in normal epithelium of the oral cavity. Most of the human non-neoplastic tissues adjacent to tumors (adjacent normal epithelium) expressed moderate amounts of the tumor suppressor PTEN (Figure 1*A*). PTEN expression was observed primarily localized to the proliferative basal layer of the epithelium (data not shown). These observations are align with our previous report in which epithelium adjacent to the tumor displayed up-regulation of PTEN [18], suggesting that these cells increase the expression of the tumor suppressor PTEN as an early protective response during transformation. However, many dysplasias (Figure 1*A*) and HNSCC invading tumor cells displayed PTEN down-regulation (Figure 1*A*, dysplasia, and insert, WD_HNSCC), which are specially observed in the areas of epithelial invasion into the surrounding stroma, indicating that PTEN may be regulated by the interaction of the cancer cells with the tumor microenvironment. Indeed, although some HNSCCs have elevated expression of PTEN (Figure 1*A*, WD_HNSCC), the carcinoma invasive front displays down-regulation of PTEN (as previously reported by us in [14]). We also observed that among the cases studied, a selected group of HNSCC patients displayed PTEN down-modulation throughout the tumor lesion (Figure 1, *A*–*C*). We also took advantage of available databases to analyze whether PTEN expression in primary tumors inversely correlates with lymph node spread. Indeed, the involvement of lymph nodes in HNSCC patients is associated with reduced expression of *PTEN* (Figure 1*D*; $^{***}P \leq .001$). This suggests that *PTEN* down-regulation may have prognostic significance, as lymph node invasion correlates with low disease-free survival and poor overall prognosis of HNSCC patients [25].

PTEN Down-Regulation Is Present in 30% of HNSCCs and Correlates with the Activation of PI3K/AKT/mTOR Pathway in HNSCC Patients

We next analyzed multiple HNSCC lesions (NIDCR, $n = 347$ cores; University of Chicago, $n = 362$ cores) among four TMAs by immunohistochemistry (IHC) using anti-PTEN antibody. First, all normal oral epithelia (100%, $n = 10$) were positive for PTEN, which showed at least 80% of the cells staining positively within the epithelial basal layer (Figure 1*B*). In this large number of HNSCC cases, however, we established that 31.2% of HNSCCs displayed down-modulation of PTEN protein levels (Figure 1*B*, $n = 709$, $^{**}P < .01$ *vs* normal controls), as seen in representative examples of positive and negative PTEN stainings in the selected TMA cores of HNSCC (Figure 1*C*). Detailed analysis of the HNSCC TMAs showed distinct immunoreactivity for PTEN, according to the scoring of positive cells that range from score 0 (10% positive cells) to 4 (100% positive cells; Figure 2*A*). Interestingly, lower average PTEN scores were closely related with poorly differentiated HNSCC cases (1.30 ± 0.17), but no differences were observed in the average staining score for well-differentiated (2.17 ± 0.14) and mid-differentiated (2.18 ± 0.15) carcinomas (Figure 2*B*). Next, we evaluated the relationship between expression levels of PTEN and the status of a number of key molecules of the PI3K/AKT/mTOR pathway and important markers associated with HNSCC prognosis and treatment,

including p53, EGFR, and its phosphorylated active form (pEGFR). The multiple TMAs allowed us to survey hundreds of tumor tissues for all the selected markers simultaneously. The results were analyzed by unsupervised hierarchical clusters based on the similarities of the seven biomarkers. The cluster analysis was done only in samples that had staining of at least four of the seven markers used. Approximately 310 data points (HNSCC samples) were included in the analysis and plotted in a heat map (Figure 2*C*). Tissue scores were represented as follows: 0, green; 1, black; 2, dark red; 3, medium red; 4, bright red. No available data were represented as gray. The heat map displayed the expression of proteins and phosphoproteins (Figure 2*C*, *right*) in relation to HNSCC (Figure 2*C*, *top*). As expected, $pAKT^{Ser473}$, pS6, $pAKT^{Thr308}$, and PTEN clustered together, and interestingly, EGFR was part of this cluster division. However, p53 and pEGFR were clustered separately from these markers. Of note, some tissue clusters became evident. The cluster depicted as A in Figure 2*C* showed samples negative for both PTEN and pEGFR, while the cluster represented as A1 included tumors positive for PTEN and pEGFR simultaneously.

A Genetically Defined Oral HNSCC Animal Model Was Generated by Combining Intraoral Excision of the Tumor Suppressor Pten and Local Administration of the Tobacco Surrogate 4NQO, Which Resulted to HNSCC Tumor Formation in the Oral Cavity

Pten was conditioned deleted from the epithelial compartment by crossing mice harboring a floxed *Pten* allele ($Pten^{F/F}$) with mice expressing the Cre recombinase under the control of the K14 promoter (K14Cre). Effective gene excision in epithelial cells of the tongue and oral mucosa was confirmed by K14Cre/ROSA-floxed-lacZ mice, which displayed positivity for β-galactosidase seen in blue (Figure 3*A*). Next, as seen in Figure 3*B*, mice harboring *Pten* deletion (K14Cre $Pten^{F/+}$ and K14Cre $Pten^{F/F}$) and control mice were exposed to vehicle

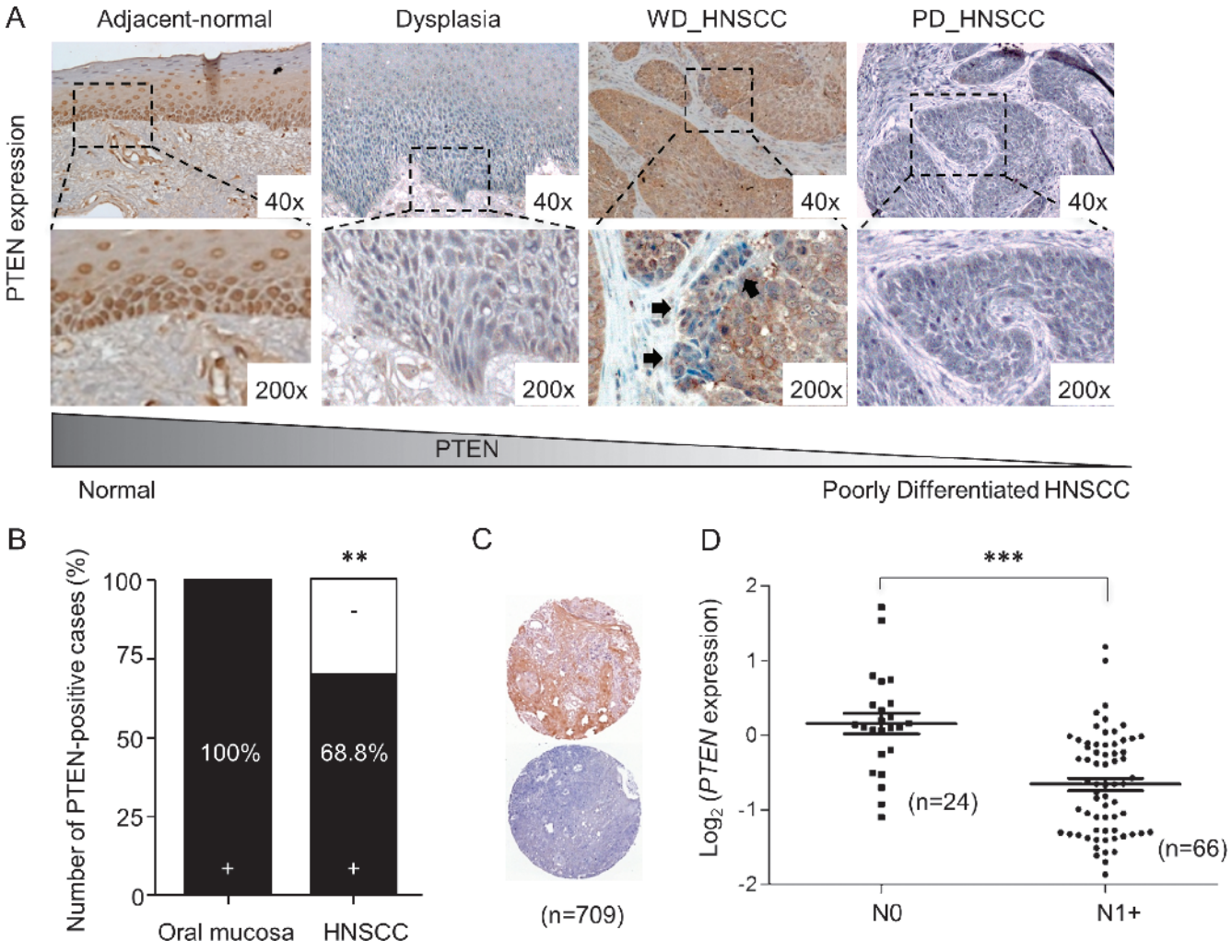

Figure 1. Loss of PTEN during tumor transformation and lymph node involvement. (A) Representative examples of PTEN expression in normal, dysplastic, and HNSCC from humans demonstrating PTEN expression. Note PTEN down-regulation in the dysplastic epithelium and in the HNSCC epithelial cell invasion (black arrows). (B) Analysis of PTEN expression on oral epithelia ($n = 10$) and four TMAs for HNSCC (containing $n = 709$). In normal oral epithelia, PTEN staining was positive mostly in the basal layer. Note an overall PTEN loss in 31.2% of all HNSCC tumors (**$P < .01$). (C) Representative examples of PTEN staining in HNSCC TMA tumor core ($n = 709$; positive, top; negative, bottom). (D) Scatter plot of relative microarray signal intensities for *PTEN* mRNA in HNSCC samples from patients with negative lymph nodes (N0) *versus* presence of lymph node metastases (N1+; error bar, SEM; **$P \leq .01$; ***$P \leq .001$).

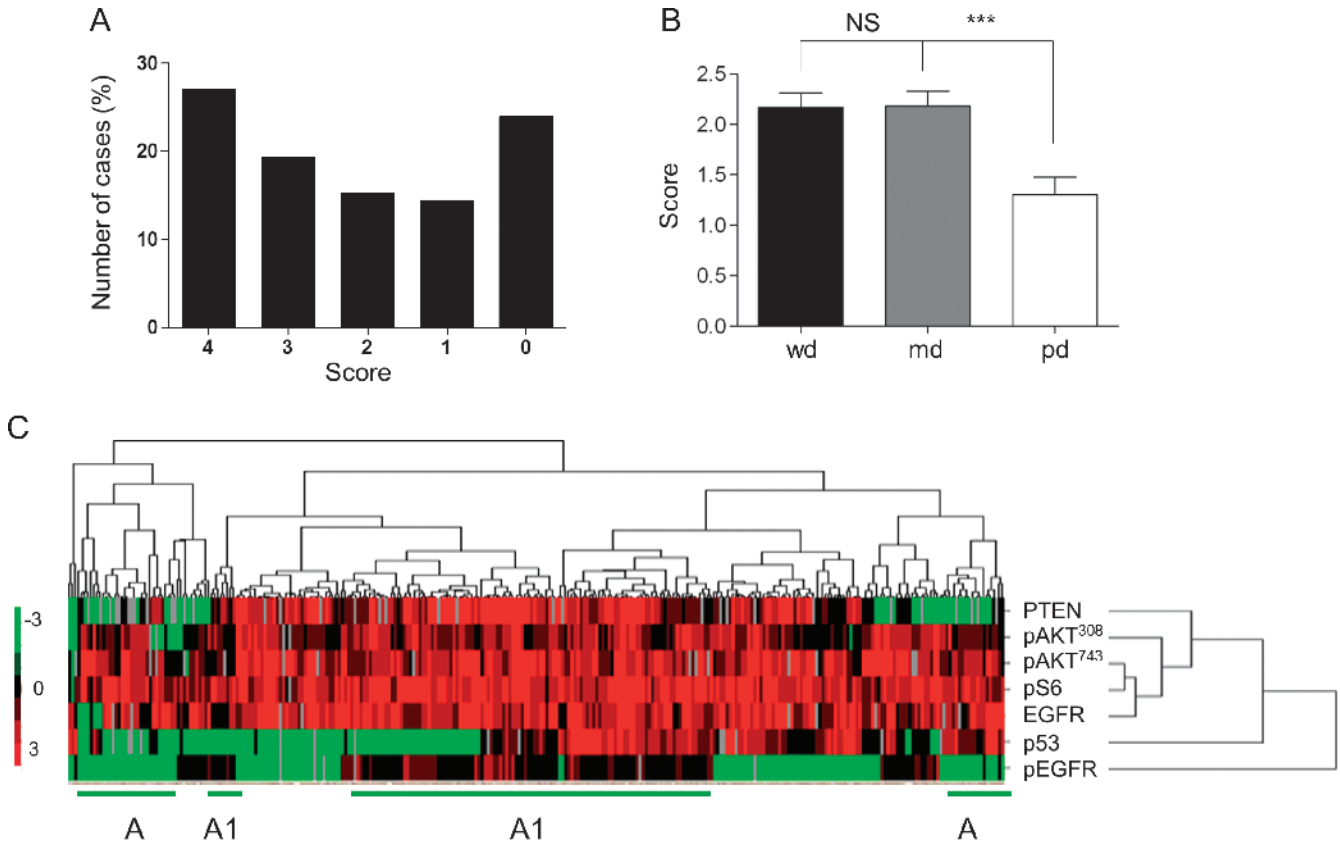

Figure 2. Evaluation for PTEN and proteins in the PI3K/mTOR pathways in HNSCC samples. (A) HNSCC TMA slides (NIDCR) were analyzed for PTEN (IHC). PTEN immunoreactivity in the tissue array cores ($n = 347$) was classified into five groups: 0 (less than 10% stained cells), 1 (10–25%), 2 (25–50%), 3 (50–75%), and 4 (75–100%). (B) PTEN levels in well-differentiated (wd), moderately differentiated (md), and poorly differentiated (pd) tumors. Scores were represented as average of PTEN stain per differentiation group (error bar, SEM; $***P \leq .001$). Poorly differentiated tumors (pd) express significantly lower levels of PTEN than well-differentiated (wd) or moderately differentiated carcinomas (md). (C) Heat map generated from the IHC analysis of the indicated proteins in the tissue microarray. Unsupervised clustering analysis shows correlation between $pAKT^{Ser473}$, pS6, EGFR, $pAKT^{Thr308}$, and PTEN. Separation of clusters was indicated for the groups in which PTEN and pEGFR are co-expressed (A), whereas cluster A1 defines a subgroup of HNSCC lesions in which both proteins are decreased.

or 4NQO, a tobacco surrogate that forms DNA adducts, substitutions in adenosine for guanosine, oxidative stress, DNA breaks, and mutations, typical from those provoked by tobacco carcinogen [26–28]. Treatment started after weaning and continues for 13 weeks. At the end of the study, mice were euthanized and tissue was collected. As expected, none of the control and K14Cre $Pten^{F/+}$ mouse groups treated with the vehicle in the drinking water developed lesions at the end of the study (Figure 3*C*, control). Gross examination of K14Cre $Pten^{F/F}$ mice from the vehicle-treated group displayed multiple lesions (Figures 3, *D* and *E*, and 4*A*, K14Cre $Pten^{F/F}$/vehicle), which were small white patches clinically similar to leukoplakias. Notably, leukoplakias are white lesions that have been associated with a higher risk of transformation, mostly present in adults more than 40 years of age, and cancer prevalence increases rapidly with age [29,30]. These observations may indicate that PTEN down-modulation predisposes the oral epithelium to transformation. Here, we chose to work with BALB/c mice, a strain shown to be resistant to the carcinogenic effects of 4NQO [26], hence providing a more sensitive biologic system to explore the contribution of Pten. Indeed, control mice did not develop lesions throughout the study (Figure 3*C*, control). However, our model combining *Pten* deletion with 4NQO treatment allowed us to determine specific contribution of PTEN down-modulation and subsequent PI3K/mTOR activation to HNSCC. Remarkably, K14Cre $Pten^{F/+}$ and K14Cre $Pten^{F/F}$ mice developed lesions as early as in 6 weeks of 4NQO exposure. Most of the lesions developed as irregular growth ranging from white appearance to ulcerated lesions on the lateral border and ventral part of the tongue and floor of the mouth (Figure 3, *C* and *D*), which are some of the most common sites of intraoral carcinomas in humans. Of note, K14Cre $Pten^{F/F}$ mice exposed to 4NQO also displayed widespread dysplastic white lesions on the dorsal, ventral, and lateral borders of the tongue (Figure 3, *C* and *D*), which resemble the "field cancerization" that is often associated with tobacco exposure and higher risk of developing multiple carcinomas in humans [2,4,31,32].

The Pten/4NQO Animal Model Recapitulates HNSCC Development and Progression and Displays PI3K/mTOR Activation

The number and size of the intraoral tumors from mice displaying Pten down-modulation continued to grow progressively even after the removal of 4NQO from the drinking water (Figure 3, *E* and *F*). Overall, these mice developed one or more large intraoral tongue lesions (Figure 3*F*; $P \leq .001$). Indeed, clinical visible lesions of the tongue

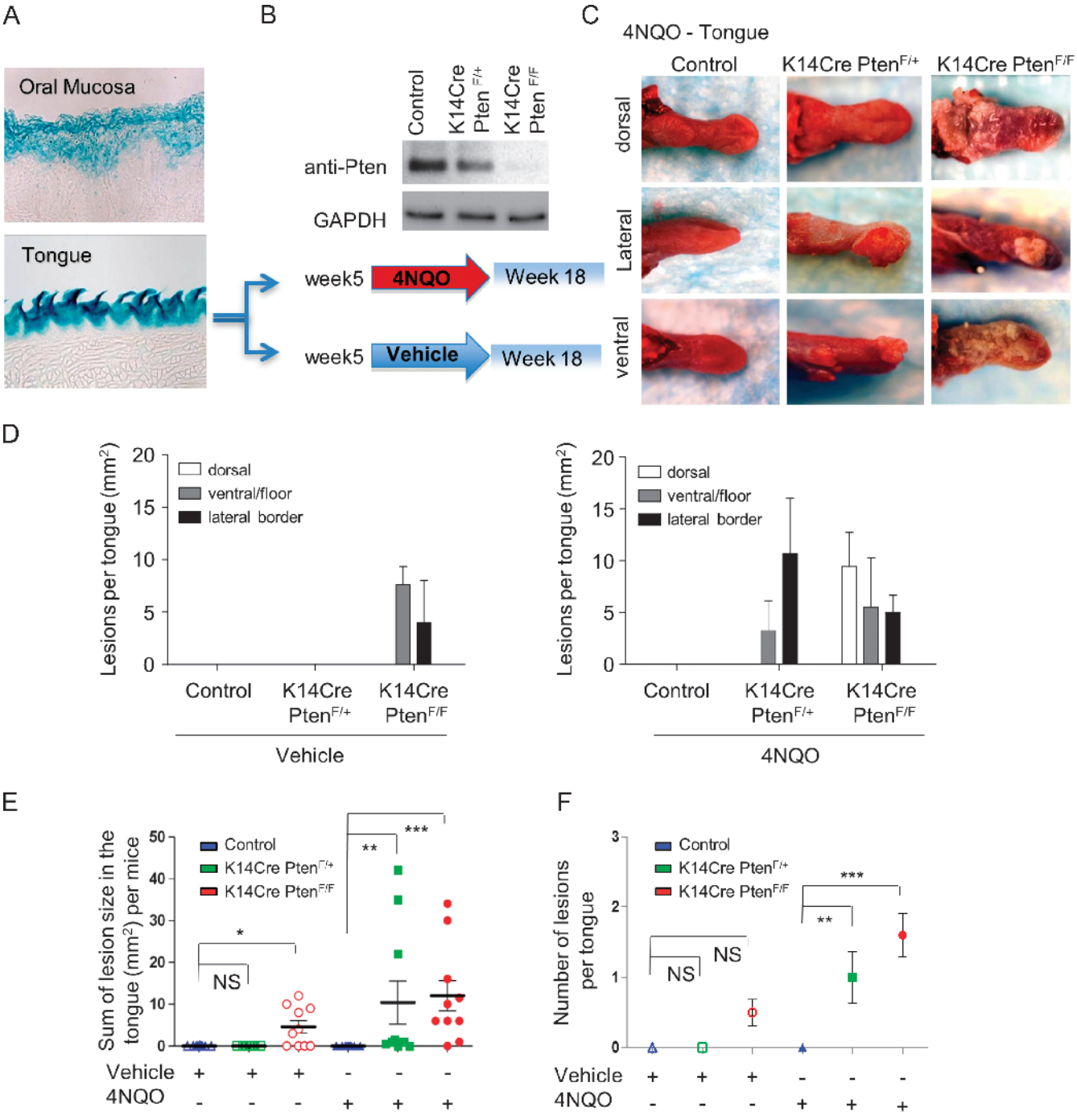

Figure 3. Loss of *Pten* combined with 4NQO exposure promotes oral tumor formation. (A) Detection of gene deletion in blue (β-galactosidase activity assay) driven by the K14Cre promoter is seen in the epithelial cells from mouse oral mucosa and tongue. (B) The immunoblot shows reduced or absent levels of Pten in epithelial cells in primary keratinocyte cultures isolated from K14Cre Pten$^{F/+}$ and K14Cre Pten$^{F/F}$ mice. Glyceraldehyde 3-phosphate dehydrogenase (GAPDH) was used as a loading control. Control, K14Cre Pten$^{F/+}$, and K14Cre Pten$^{F/F}$ mouse groups (n = 10 per group) started treatment with vehicle or 4NQO in drinking water after weaning (~5-week-old mice). Mice were killed on week 18. (C) The tongue of each mouse was examined grossly and histologically as described in Materials and Methods section. Representative photographs of lesion on the dorsum, lateral border, and ventral part of the tongue are seen for each 4NQO treatment group and control. No gross changes were observed in untreated control mice. Elevated white lesions and tumor masses, often ulcerated, were found in K14Cre Pten$^{F/+}$ and K14Cre Pten$^{F/F}$ mice treated with 4NQO. (D) The average lesion size experimental group (control, K14Cre Pten$^{F/+}$, and K14Cre Pten$^{F/F}$) is depicted according to their anatomic location in the tongue, ventral/floor, and lateral border, for vehicle and 4NQO treatments. (E) The average size in mm^2 of lesions per mouse is shown for each experimental group. Dots represent the sum of all lesions in each mouse tongue. (F) Tumor multiplicity is shown as the average of number of lesions per experimental group treated with vehicle and 4NQO (error bar, SEM; *$P \leq .05$, **$P \leq .01$, ***$P \leq .001$, and NS, not significant).

in K14Cre Pten$^{F/+}$ and K14Cre Pten$^{F/F}$ animals had an average size of 10.4 ± 5.1 and 12.0 ± 3.6 mm^2, respectively (Figure 3*E*). As expected, control and K14Cre Pten$^{F/+}$ mice treated with the vehicle did not develop lesions at the end of the study. Of interest, 50% of the mice with deletion of both alleles of *Pten*, K14Cre Pten$^{F/F}$, displayed multiple small leukoplakias throughout the oral mucosa and tongue, which together affected an average of 4.6 ± 1.5 mm^2 per mouse (Figure 3*E*, vehicle). Histologically, control animals displayed a normal keratinized stratified squamous epithelium forming the tongue papillae (Figure 4, *A* and *C*, vehicle/control). Half of K14Cre Pten$^{F/+}$ mice displayed epithelial changes (hyperplasia) such as a discrete increase in keratin expression and in the thickness of the epithelial layers (Figure 4, *A* and *C*, vehicle/K14Cre Pten$^{F/+}$). K14Cre Pten$^{F/F}$ mice displayed multiple hyperplastic and dysplastic lesions. Histologic analysis displayed hyperchromatic (darkening of) nuclei, enlargement of the epithelial layers including the spinous layer (acanthosis), premature keratinization of cells (dyskeratosis), loss of progressive maturation or epithelial layer toward the surface (loss of epithelium polarity), and an enlarged keratin surface (hyperkeratosis), which are aligned with the clinical observations of leukoplakias in these mice (Figure 4, *A* and *C*, vehicle/K14Cre Pten$^{F/F}$). Although clinical changes on the surface of the tongue could not be observed in the control mice under 4NQO treatment, most likely because the keratin thickness was not changed, histologically 20% of the mice displayed hyperplasia-associated changes in the epithelial maturation and increased thickness of the spinous and granulous layers (acanthosis; Figure 4, *B* and *C*, 4NQO/control). At the end of the treatment, all K14Cre Pten$^{F/+}$ and K14Cre Pten$^{F/F}$ mice displayed abnormal epithelial changes that ranged from hyperplasia to carcinomas (Figure 4, *B* and *C*). All malignant tumors were identified with different degrees of keratinization and angiogenesis. Multiple malignant epithelial cells formed invasive masses of islands and cords. A small percentage of K14Cre Pten$^{F/+}$ mice presented only hyperplasias (20%) or potential precancerous lesions (dysplasias; 20%). Approximately 60% of these mice exhibited invasive and aggressive squamous cell carcinomas. However, all K14Cre Pten$^{F/F}$ mice exposed to 4NQO displayed multiple or extensive dysplasias, and 100% of these mice presented with squamous cell carcinomas, which ranged from *in situ* to superficially and deeply invasive carcinomas (Figure 4*C*).

Because PI3K/mTOR signaling is frequently upregulated in patients with HNSCC, we next investigated the activation status of this pathway in our HNSCC carcinogenesis model in hyperplastic, dysplastic, and tumor lesions. Lesions were stained for pS6, a well-defined biomarker used in preclinical and clinical studies to establish mTOR activation [33]. Initially, we found few positive cells close to the surface of the tongue epithelium of control mice (Figure 4*A*, control/vehicle and 4NQO). The positive cells were in the granular layer, a nonproliferative and more differentiated keratinocyte compartment. mTOR activation, as judged as pS6 accumulation, increased upon 4NQO treatment, which expanded along the hyperplastic lesions. Interesting, a progressive dysregulation of PI3K/mTOR pathway was observed. Hyperplastic and dysplastic lesions of K14Cre Pten$^{F/+}$ and K14Cre Pten$^{F/F}$ mice also displayed mTOR activation, which were further accentuated by 4NQO treatment (Figure 4, *A* and *B*). The increased expression of pS6 gradually expanded toward the spinous, suprabasal, and basal layers, which were absent in control animals (Figure 4*B*). Furthermore, tumors in our animal model presenting Pten deletion showed multifocal areas of mTOR activation throughout the tumor (Figure 4*B*, tumors).

Pten Down-Regulation Leads to Augmented Angiogenesis and Increased COX-2 Expression and Does Not Require the Expression of Mutant p53

In addition to the direct impact of Pten down-regulation on the squamous epithelial cells, we next explored whether decreased Pten expression could alter the microenvironment in which the SCC tumors arise. We studied the effects of Pten deregulation in angiogenesis by analyzing the number of blood vessels present in the tongue of mice with Pten deregulation. As seen in Figure 5*A*, the density of blood vessels increased following *Pten* deletion, indicating that Pten deregulation in epithelial cells can promote a cross talk between epithelial and stromal cells to create a specific niche more susceptible to tumor formation. COX-2 has been shown to be unregulated in HNSCC and to participate in tumor angiogenesis and tumor progression [34–36]. Here, we found that in control animal exposed to 4NQO, COX-2 expression was found confined to the connective tissue. However, COX-2 expression was found in dysplastic epithelial cells as well in oral tumors upon Pten down-modulation. Indeed, Pten deletion was sufficient to cause increased angiogenesis in the surrounding stroma, and tumors arising in conditional *Pten* mice exhibited increased levels of the proinflammatory molecule COX-2, even in dysplastic lesions. Thus, decreased PTEN levels in tumor tissues may initiate an angiogenic and proinflammatory process in the surrounding oral mucosa. Next, we analyzed p53 expression. p53 was found not to be expressed in Pten-dependent dysplasias and oral tumors, suggesting that PTEN down-regulation may circumvent the requirement of p53 mutations. This is aligned with the fact that many human tumors displaying reduced PTEN levels do not exhibit accumulation of p53, often reflecting the presence of mutations in its encoding gene. As expected, we also observed increased phosphorylation of AKT, using pAKT^{Ser473} as readout, in dysplastic and tumor lesions in mice in which the *Pten* gene was conditionally deleted, aligned with the increased activation of this signaling molecule and the mTOR pathway in human HNSCC tissues. Altogether, these findings provide a strong rationale for further clinical and preclinical studies with mTOR inhibitors to prevent and treat HNSCC. Furthermore, because a subset of patients may present higher PI3K/mTOR activation as a consequence of PTEN mutations and inactivation, PI3K and TSC1/2 mutations, these patients could potentially benefit the most from this targeted therapy.

Discussion

In this study, we investigated the potential ability of combining two major players in HNSCC formation to engineer an animal model for intraoral HNSCC capable of recapitulating the fundamental genetic and biologic characteristics of HNSCC tumors. Specifically, the carcinogenic potential of tobacco was studied here by the administration of its chemical surrogate, 4NQO, and associated with the selective up-regulation of a growth-promoting pathway represented by PI3K/mTOR. Most HNSCC patients present key genetic and epigenetic alterations that lead to aberrant gene and protein expression. Along mutations in the *p53* and *Notch* genes, activating mutations in the *PIK3CA* gene, often referred to as the *PIK3CA* oncogene, results in constitutive activation of AKT and downstream proteins such as mTOR [5,6,37,38]. Furthermore, AKT is known to be activated in the majority of HNSCC tumor tissue and cell lines [18,39], and its active form is detected in 50% of preneoplastic lesions [40]. The activation of this pathway is caused by multiple genetic and epigenetic events in HNSCC, including mutations in the *RAS* and *PIK3KCA* oncogenes, as well as by

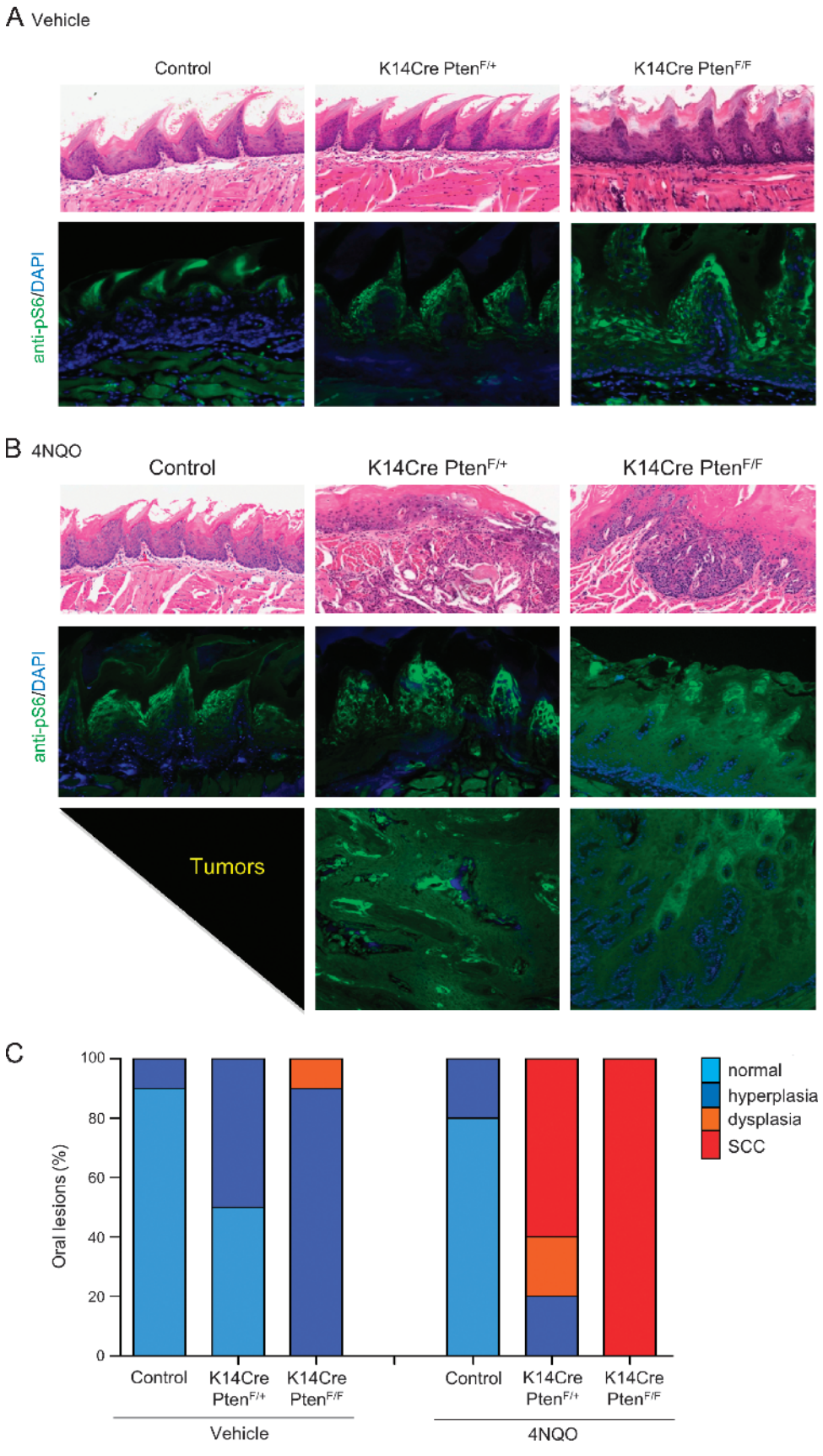
A Vehicle
Control
K14Cre PtenF/+
K14Cre PtenF/F
anti-pS6/DAPI
B 4NQO
Control
K14Cre PtenF/+
K14Cre PtenF/F
anti-pS6/DAPI
Tumors
C
Oral lesions (%)
100
80
60
40
20
0
normal
hyperplasia
dysplasia
SCC
Control
K14Cre PtenF/+
K14Cre PtenF/F
Control
K14Cre PtenF/+
K14Cre PtenF/F
Vehicle
4NQO

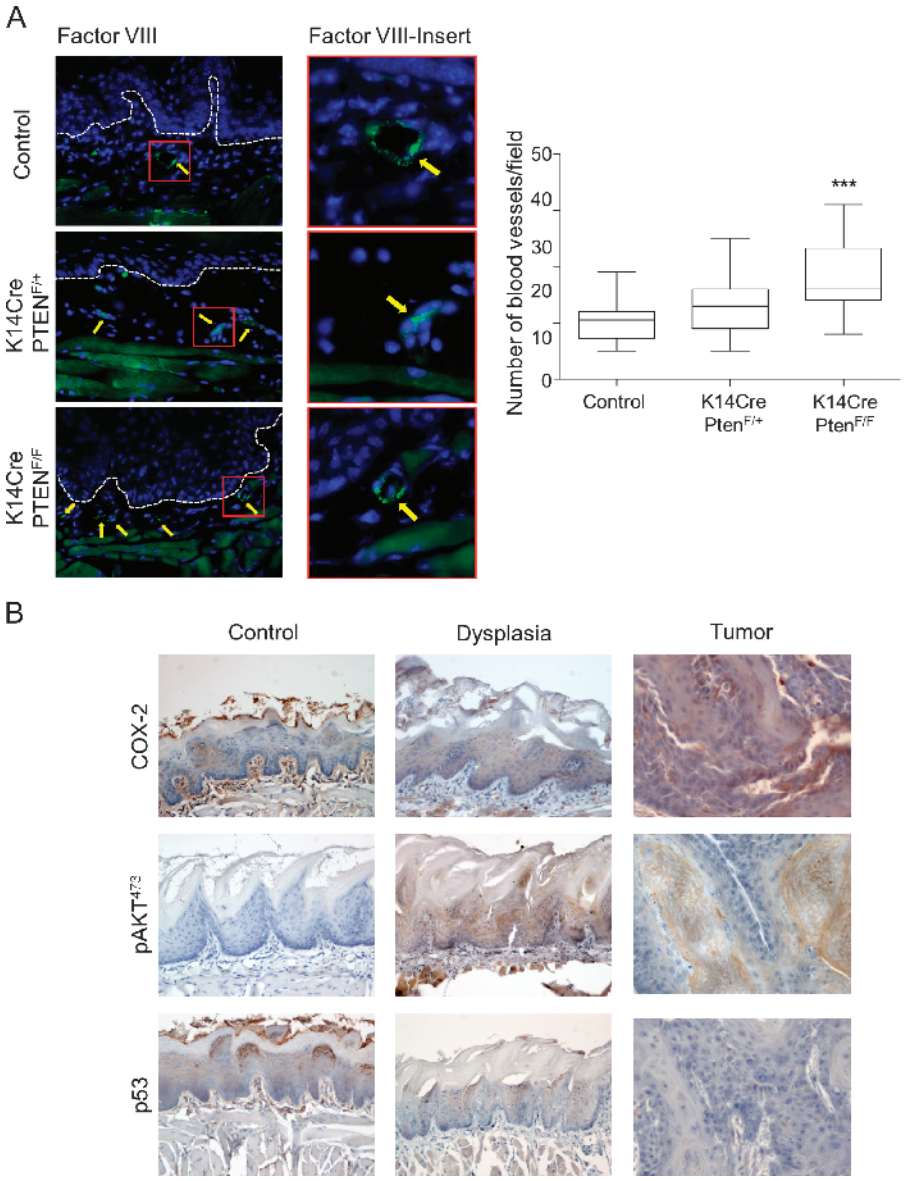

Figure 5. Pten deletion induces angiogenesis and up-regulation of pAKT activity and COX-2 expression in epithelial dysplasias and oral tumors. (A) Blood vessel density was detected by factor VIII staining and defined as number of blood vessels per field. Micrographs are representative examples of blood vessels stained with factor VIII (arrow) in oral tissue from control, K14Cre Pten$^{F/+}$, and K14Cre Pten$^{F/F}$ mice (***$P < .001$). (B) Oral dysplasias and tumors induced by the tobacco surrogate (4NQO) with Pten deregulation (K14Cre Pten$^{F/F}$) display up-regulation of pAKT^{Ser473} and COX-2, the latter in both the epithelial cells and the tumor stroma, and do not involve the accumulation of mutant p53.

Figure 4. Gradual loss of Pten leads to increased number of carcinomas in the oral cavity after exposure to 4NQO. The tongue of every mouse from control, K14Cre Pten$^{F/+}$, and K14Cre Pten$^{F/F}$ groups ($n = 10$ per group) was processed for histologic examination as described in Materials and Methods section. Representative histologic pictures (H&E stain) of each group of mice treated with vehicle (A) and 4NQO (B) are depicted. (A) Representative example of tongue histologic section from control mice (vehicle treated) displaying normal histologic features. Hyperplasia and dyskeratosis are common features of K14Cre Pten$^{F/+}$. K14Cre Pten$^{F/F}$ dysplastic changes such as hyperchromatic nuclei, acanthosis, dyskeratosis, loss of epithelium polarity, and hyperkeratosis (see text for details) were also seen. Positive immunoreactivity of the mTOR downstream target pS6 in normal tissues is limited to the upper layers of the squamous epithelium of the dorsal tongue (control/vehicle). Increased expression of pS6 is found on K14Cre Pten$^{F/+}$ and K14Cre Pten$^{F/F}$ mouse tissues. Most keratinocytes from K14Cre Pten$^{F/F}$ mice displayed pS6 expression regardless of their differentiation stage. (B) Exposure to the carcinogen (4NQO) induced moderate histologic changes in control mice (hyperplasia and dyskeratosis). K14Cre Pten$^{F/+}$ and K14Cre Pten$^{F/F}$ developed carcinomas in the tongue. Dysregulated activation of mTOR (shown by pS6 expression) is found in all mouse groups treated with 4NQO. pS6 immunoreactivity is further increased by the *Pten* ablation (as seen in K14Cre Pten$^{F/+}$ and K14Cre Pten$^{F/F}$). The lower photographs show high up-regulation of mTOR activity (pS6 expression) in tumors with *Pten* ablation (left, K14Cre Pten$^{F/+}$; right, K14Cre Pten$^{F/F}$). (C) Normal, hyperplasia, dysplasias (preneoplastic lesions), and carcinomas were evaluated in histologic slides from the tongue of each animal. The results are expressed as percentage of the total changes in each experimental group.

EGFR overexpression and by the expression of constitutively activated truncated mutant forms of EGFR, EGFRvIII [41].

In general, the molecular events responsible for AKT/mTOR activation involves PI3K activation, which promotes PIP_3 synthesis by phosphorylating PIP_2 in the 3 position of the inositol ring at the cell membrane, which in turn promotes AKT phosphorylation. PTEN is a lipid phosphatase that directly opposes PI3K by dephosphorylating PIP_3 and thus inhibits its downstream signaling [11,12,42,43]. Therefore, PTEN is responsible for blocking the PI3K pathway, and PTEN inactivation or deletion mimics activating PI3K/AKT/mTOR pathway mutations and epigenetic alterations [44]. Moreover, underscoring PTEN contribution to HNSCC, *PTEN* gene has been shown to be mutated in 8% to 23% of HNSCCs [6–8], and as shown here, PTEN protein is absent or downregulated in approximately 30% of HNSCC cases. Furthermore, the lack of PTEN expression often results in aggressive tumors, which is reflected by PTEN association to poor disease-free and overall survival [44].

In vivo studies of important genes involved in HNSCC are mostly accomplished using transgenic animal models engineered to target the expression of a variety of oncogenes in the epidermis, which result in the development of papillomas and carcinomas in the skin [45–48]. Some animal models also rely in the addition of 7,12-dimethylbenz[α]anthracene (DMBA)/12-O-tetradecanoyl-phorbol-13-acetate (TPA), which involves the activation of *RAS*, an important component often found in a subset of tumors in Asia associated with the use of areca nut [49]. These multistage animal models result in the formation of papillomas that further progress to full-blown carcinomas in a process rarely observed in Western HNSCC [50–52]. Here, we combined the intraoral administration of a tobacco surrogate, 4NQO, with the conditional deletion of the *Pten* gene using *Pten* floxed mice. This resulted in overactivity of PI3K/AKT/mTOR caused by Pten ablation from the proliferative layer of the oral mucosa using the CRE-lox system under the keratin promoter 14. This provided a specific genetic and environmentally defined animal model for HNSCC that resulted in the development of oral specific carcinomas. Remarkably, most of the tumors arose in the lateral border and ventral part of the tongue and floor of the mouth, which are preferred anatomic sites for human HNSCC. Furthermore, the presence of malignant carcinomas in the animal cohort bearing both deficiency for Pten and 4NQO administration argues that combined factors, such as epigenetic events resulting in reduced PTEN levels or genetic alterations in its coding gene, together with tobacco exposure, can cause tumors to arise and to progress to a fully malignant state, often in a multifocal fashion.

Overall, our study highlights the likely clinical relevance of reduced PTEN expression and/or inactivation in HNSCC progression. In addition, the intraoral tumors arising in our genetically defined HNSCC animal model closely mimic the histology and etiology of human HNSCC often found in tobacco users, presenting similar progression pattern and activated pathways. Thus, the combined *Pten* deletion with exposure to tobacco carcinogens or their surrogates may provide a unique model system to study novel molecular target treatments for HNSCC patients.

References

[1] Siegel R, Naishadham D, and Jemal A (2012). Cancer statistics, 2012. *CA Cancer J Clin* **1**, 10–29.

[2] Day GL, Blot WJ, Shore RE, McLaughlin JK, Austin DF, Greenberg RS, Liff JM, Preston-Martin S, Sarkar S, and Schoenberg JB (1994). Second cancers following oral and pharyngeal cancers: role of tobacco and alcohol. *J Natl Cancer Inst* **2**, 131–137.

[3] D'Souza G, Kreimer AR, Viscidi R, Pawlita M, Fakhry C, Koch WM, Westra WH, and Gillison ML (2007). Case-control study of human papillomavirus and oropharyngeal cancer. *N Engl J Med* **19**, 1944–1956.

[4] Slaughter DP, Southwick HW, and Smejkal W (1953). Field cancerization in oral stratified squamous epithelium; clinical implications of multicentric origin. *Cancer* **5**, 963–968.

[5] Agrawal N, Frederick MJ, Pickering CR, Bettegowda C, Chang K, Li RJ, Fakhry C, Xie T-X, Zhang J, Wang J, et al. (2011). Exome sequencing of head and neck squamous cell carcinoma reveals inactivating mutations in *NOTCH1*. *Science* **6046**, 1154–1157.

[6] Stransky N, Egloff AM, Tward AD, Kostic AD, Cibulskis K, Sivachenko A, Kryukov GV, Lawrence MS, Sougnez C, McKenna A, et al. (2011). The mutational landscape of head and neck squamous cell carcinoma. *Science* **6046**, 1157–1160.

[7] Poetsch M, Lorenz G, and Kleist B (2002). Detection of new *PTEN/MMAC1* mutations in head and neck squamous cell carcinomas with loss of chromosome 10. *Cancer Genet Cytogenet* **1**, 20–24.

[8] Shao X, Tandon R, Samara G, Kanki H, Yano H, Close LG, Parsons R, and Sato T (1998). Mutational analysis of the *PTEN* gene in head and neck squamous cell carcinoma. *Int J Cancer* **5**, 684–688.

[9] Saal LH, Holm K, Maurer M, Memeo L, Su T, Wang X, Yu JS, Malmström P-O, Mansukhani M, Enoksson J, et al. (2005). *PIK3CA* mutations correlate with hormone receptors, node metastasis, and ERBB2, and are mutually exclusive with PTEN loss in human breast carcinoma. *Cancer Res* **7**, 2554–2559.

[10] Thomas RK, Baker AC, DeBiasi RM, Winckler W, LaFramboise T, Lin WM, Wang M, Feng W, Zander T, MacConaill L, et al. (2007). High-throughput oncogene mutation profiling in human cancer. *Nat Genet* **3**, 347–351.

[11] Maehama T and Dixon JE (1998). The tumor suppressor, PTEN/MMAC1, dephosphorylates the lipid second messenger, phosphatidylinositol 3,4,5-trisphosphate. *J Biol Chem* **22**, 13375–13378.

[12] Stambolic V, Suzuki A, de la Pompa JL, Brothers GM, Mirtsos C, Sasaki T, Ruland J, Penninger JM, Siderovski DP, and Mak TW (1998). Negative regulation of PKB/Akt-dependent cell survival by the tumor suppressor PTEN. *Cell* **1**, 29–39.

[13] Squarize CH, Castilho RM, and Gutkind JS (2008). Chemoprevention and treatment of experimental Cowden's disease by mTOR inhibition with rapamycin. *Cancer Res* **17**, 7066–7072.

[14] Squarize CH, Castilho RM, Bugge TH, and Gutkind JS (2010). Accelerated wound healing by mTOR activation in genetically defined mouse models. *PloS One* **5**, e10643.

[15] Czerninski R, Amornphimoltham P, Patel V, Molinolo AA, and Gutkind JS (2009). Targeting mammalian target of rapamycin by rapamycin prevents tumor progression in an oral-specific chemical carcinogenesis model. *Cancer Prev Res (Phila)* **1**, 27–36.

[16] Soriano P (1999). Generalized lacZ expression with the ROSA26 Cre reporter strain. *Nat Genet* **1**, 70–71.

[17] Squarize CH, Castilho RM, and Santos Pinto D Jr (2002). Immunohistochemical evidence of PTEN in oral squamous cell carcinoma and its correlation with the histological malignancy grading system. *J Oral Pathol Med* **7**, 379–384.

[18] Molinolo AA, Hewitt SM, Amornphimoltham P, Keelawat S, Rangdaeng S, Meneses García A, Raimondi AR, Jufe R, Itoiz M, Gao Y, et al. (2007). Dissecting the Akt/mammalian target of rapamycin signaling network: emerging results from the head and neck cancer tissue array initiative. *Clin Cancer Res* **17**, 4964–4973.

[19] Rhodes DR, Kalyana-Sundaram S, Mahavisno V, Varambally R, Yu J, Briggs BB, Barrette TR, Anstet MJ, Kincead-Beal C, Kulkarni P, et al. (2007). Oncomine 3.0: genes, pathways, and networks in a collection of 18,000 cancer gene expression profiles. *Neoplasia* **2**, 166–180.

[20] Ginos MA, Page GP, Michalowicz BS, Patel KJ, Volker SE, Pambuccian SE, Ondrey FG, Adams GL, and Gaffney PM (2004). Identification of a gene expression signature associated with recurrent disease in squamous cell carcinoma of the head and neck. *Cancer Res* **1**, 55–63.

[21] Cromer A, Carles A, Millon R, Ganguli G, Chalmel F, Lemaire F, Young J, Dembélé D, Thibault C, Muller D, et al. (2004). Identification of genes associated with tumorigenesis and metastatic potential of hypopharyngeal cancer by microarray analysis. *Oncogene* **14**, 2484–2498.

[22] Chung CH, Parker JS, Karaca G, Wu J, Funkhouser WK, Moore D, Butterfoss D, Xiang D, Zanation A, Yin X, et al. (2004). Molecular classification of head

and neck squamous cell carcinomas using patterns of gene expression. *Cancer Cell* **5**, 489–500.

[23] O'Donnell RK, Kupferman M, Wei SJ, Singhal S, Weber R, O'Malley B, Cheng Y, Putt M, Feldman M, Ziober B, et al. (2005). Gene expression signature predicts lymphatic metastasis in squamous cell carcinoma of the oral cavity. *Oncogene* **7**, 1244–1251.

[24] Castilho RM, Squarize CH, Leelahavanichkul K, Zheng Y, Bugge T, and Gutkind JS (2010). Rac1 is required for epithelial stem cell function during dermal and oral mucosal wound healing but not for tissue homeostasis in mice. *PloS One* **5**, e10503.

[25] Lee JI, Soria JC, Hassan KA, El-Naggar AK, Tang X, Liu DD, Hong WK, and Mao L (2001). Loss of PTEN expression as a prognostic marker for tongue cancer. *Arch Otolaryngol Head Neck Surg* **12**, 1441–1445.

[26] Vitale-Cross L, Czerninski R, Amornphimoltham P, Patel V, Molinolo AA, and Gutkind JS (2009). Chemical carcinogenesis models for evaluating molecular-targeted prevention and treatment of oral cancer. *Cancer Prev Res (Phila)* **5**, 419–422.

[27] Panigrahi GB and Walker IG (1990). The N2-guanine adduct but not the C8-guanine or N6-adenine adducts formed by 4-nitroquinoline 1-oxide blocks the 3′-5′ exonuclease action of T4 DNA polymerase. *Biochemistry* **8**, 2122–2126.

[28] Hawkins BL, Heniford BW, Ackermann DM, Leonberger M, Martinez SA, and Hendler FJ (1994). 4NQO carcinogenesis: a mouse model of oral cavity squamous cell carcinoma. *Head Neck* **5**, 424–432.

[29] Pindborg JJ, Jolst O, Renstrup G, and Roed-Petersen B (1968). Studies in oral leukoplakia: a preliminary report on the period pervalence of malignant transformation in leukoplakia based on a follow-up study of 248 patients. *J Am Dent Assoc* **4**, 767–771.

[30] Pindborg JJ, Kiaer J, Gupta PC, and Chawla TN (1967). Studies in oral leukoplakias. Prevalence of leukoplakia among 10,000 persons in Lucknow, India, with special reference to use of tobacco and betel nut. *Bull World Health Organ* **1**, 109–116.

[31] Cianfriglia F, Di Gregorio DA, and Manieri A (1999). Multiple primary tumours in patients with oral squamous cell carcinoma. *Oral Oncol* **2**, 157–163.

[32] van Oijen MG and Slootweg PJ (2000). Oral field cancerization: carcinogen-induced independent events or micrometastatic deposits? *Cancer Epidemiol Biomarkers Prev* **3**, 249–256.

[33] Sabatini DM (2006). mTOR and cancer: insights into a complex relationship. *Nat Rev Cancer* **9**, 729–734.

[34] Abrahao AC, Castilho RM, Squarize CH, Molinolo AA, dos Santos-Pinto D Jr, and Gutkind JS (2010). A role for COX2-derived PGE2 and PGE2-receptor subtypes in head and neck squamous carcinoma cell proliferation. *Oral Oncol* **46**, 880–887.

[35] Nathan CA, Leskov IL, Lin M, Abreo FW, Shi R, Hartman GH, and Glass J (2001). COX-2 expression in dysplasia of the head and neck: correlation with elF4E. *Cancer* **92**, 1888–1895.

[36] Greenhough A, Smartt HJM, Moore AE, Roberts HR, Williams AC, Paraskeva C, and Kaidi A (2009). The COX-2/PGE2 pathway: key roles in the hallmarks of cancer and adaptation to the tumour microenvironment. *Carcinogenesis* **30**, 377–386.

[37] Kozaki K, Imoto I, Pimkhaokham A, Hasegawa S, Tsuda H, Omura K, and Inazawa J (2006). PIK3CA mutation is an oncogenic aberration at advanced stages of oral squamous cell carcinoma. *Cancer Sci* **12**, 1351–1358.

[38] Murugan AK, Hong NT, Fukui Y, Munirajan AK, and Tsuchida N (2008). Oncogenic mutations of the PIK3CA gene in head and neck squamous cell carcinomas. *Int J Oncol* **1**, 101–111.

[39] Amornphimoltham P, Sriuranpong V, Patel V, Benavides F, Conti CJ, Sauk J, Sausville EA, Molinolo AA, and Gutkind JS (2004). Persistent activation of the Akt pathway in head and neck squamous cell carcinoma: a potential target for UCN-01. *Clin Cancer Res* **10**(12 pt 1), 4029–4037.

[40] Massarelli E, Liu DD, Lee JJ, El-Naggar AK, Lo Muzio L, Staibano S, De Placido S, Myers JN, and Papadimitrakopoulou VA (2005). Akt activation correlates with adverse outcome in tongue cancer. *Cancer* **11**, 2430–2436.

[41] Sok JC, Coppelli FM, Thomas SM, Lango MN, Xi S, Hunt JL, Freilino ML, Graner MW, Wikstrand CJ, Bigner DD, et al. (2006). Mutant epidermal growth factor receptor (EGFRvIII) contributes to head and neck cancer growth and resistance to EGFR targeting. *Clin Cancer Res* **17**, 5064–5073.

[42] Di Cristofano A, Pesce B, Cordon-Cardo C, and Pandolfi PP (1998). Pten is essential for embryonic development and tumour suppression. *Nat Genet* **4**, 348–355.

[43] Engelman JA, Luo J, and Cantley LC (2006). The evolution of phosphatidylinositol 3-kinases as regulators of growth and metabolism. *Nat Rev Genet* **8**, 606–619.

[44] Di Cristofano A and Pandolfi PP (2000). The multiple roles of PTEN in tumor suppression. *Cell* **4**, 387–390.

[45] Janssen K-P, Abal M, Abala M, El Marjou F, Louvard D, and Robine S (2005). Mouse models of K-*ras*-initiated carcinogenesis. *Biochim Biophys Acta* **2**, 145–154.

[46] Vitale-Cross L, Amornphimoltham P, Fisher G, Molinolo AA, and Gutkind JS (2004). Conditional expression of K-*ras* in an epithelial compartment that includes the stem cells is sufficient to promote squamous cell carcinogenesis. *Cancer Res* **24**, 8804–8807.

[47] White RA, Malkoski SP, and Wang X-J (2010). TGFβ signaling in head and neck squamous cell carcinoma. *Oncogene* **40**, 5437–5446.

[48] Lu S-L, Herrington H, and Wang X-J (2006). Mouse models for human head and neck squamous cell carcinomas. *Head Neck* **10**, 945–954.

[49] Saranath D, Chang SE, Bhoite LT, Panchal RG, Kerr IB, Mehta AR, Johnson NW, and Deo MG (1991). High frequency mutation in codons 12 and 61 of H-ras oncogene in chewing tobacco-related human oral carcinoma in India. *Br J Cancer* **4**, 573–578.

[50] Das N, Majumder J, and DasGupta UB (2000). *ras* Gene mutations in oral cancer in eastern India. *Oral Oncol* **1**, 76–80.

[51] Mao L, Hong WK, and Papadimitrakopoulou VA (2004). Focus on head and neck cancer. *Cancer Cell* **4**, 311–316.

[52] Clark LJ, Edington K, Swan IR, McLay KA, Newlands WJ, Wills LC, Young HA, Johnston PW, Mitchell R, and Robertson G (1993). The absence of Harvey ras mutations during development and progression of squamous cell carcinomas of the head and neck. *Br J Cancer* **3**, 617–620.